J. Fluid Mech. (1973), *vol.* 58, *part* 3, *pp.* 495–515
Printed in Great Britain

The critical state: a trapped wave model of vortex breakdown

By J. D. RANDALL AND S. LEIBOVICH
Upson Hall, Cornell University, Ithaca, N.Y. 14850

(Received 31 July 1972)

A model of vortex breakdown is presented and its predictions compared with the experiments of Sarpkaya (1971). The model is centred about a theory of long, weakly nonlinear waves propagating on critical flows in tubes of variable cross-section. Although the weakly nonlinear theory must be extended beyond its domain of formal validity, many of the experimentally observed features of vortex breakdown are reproduced by the model. The description of the time evolution of the flow field that is presented requires numerical calculations that are not simple, but some important conclusions may be determined by easy computations. In particular, the axial position of a breakdown may be found from a very simple equation (10).

1. Introduction and review

This paper is a continuation of our study of the interaction of slowly varying tube walls with nonlinear waves in rotating fluids (Leibovich & Randall 1973, which we hereafter denote by I). Here we direct attention to the case of *critical* flows (see I), and relate the results specifically with the occurrence of the axisymmetric form of the vortex breakdown phenomenon (see Hall 1972, which we denote by II).

The explanation of vortex breakdown is a source of some controversy, which is summarized by Hall in his review II. Hall presents each of the various proposed explanations, followed by the extent of its comparison with experimental observation and then by a criticism of the proposal. In the present section, we adopt the same format for our own work, coupled with observations on Hall's remarks when appropriate. We confine attention only to axisymmetric phenomena in tubes (a treatment of non-axisymmetric behaviour by Huang & Leibovich will be reported elsewhere). Although connexions with the leading-edge vortex breakdown can be made, they are not yet completely clear.

Proposal

Vortex breakdown is thought of as a large amplitude wave motion, analogous in some respects to a gasdynamic shock wave (not for its suddenness, but for its relation with small amplitude waves). The proposal is a development of the work of Squire (1962); of Benjamin (1962, 1967), particularly the latter paper; and, more explicitly, of Leibovich (1969, 1970). All of these papers are supported

by calculations of either infinitesimal or weakly nonlinear waves. The idea advanced here is that the small amplitude waves possible in rotating fluids are connected with waves of arbitrary amplitude that result from initial disturbances of greater strength. Pursuing the gasdynamic analogy a little, we suggest that the equations describing weakly nonlinear waves presented in I are related to the fully nonlinear problem in a way analogous to the relation of Burgers' equation to weakly nonlinear dissipative gasdynamics. Our calculations for the critical case in rotating flows suggest to us that the weakly nonlinear solutions are 'better than they should be' at representing the fully nonlinear phenomena of vortex breakdown and gasdynamic shock waves, respectively. We therefore offer the weakly nonlinear formulation as a model (not a theory) of vortex breakdown.

Comparison of proposal with experimental observation

The identification of vortex breakdown as a wave motion is in accord with all observations. Although experimental investigations have concentrated on vortex breakdowns with stabilized and nearly stationary locations, all observations show that the transient development consists of an upstream propagation from a downstream source of disturbance. Furthermore, all indications are that the region through which the propagation occurs is subcritical, and therefore can support long upstream-propagating waves. The flow upstream of a stationary vortex breakdown is supercritical (see II), and a positive (adverse) pressure gradient exists in the vortex core (II).

In the present paper, we report calculations based on the critical flow equations of I, and choose geometrical parameters and vortex data to simulate the experiments of Sarpkaya (1971, which we denote by III). The analysis requires that the velocity profiles far upstream of a breakdown position be given, as well as the tube wall shape and the kinematic viscosity. No more than one stationary breakdown (or 'trapped wave') of finite energy can then exist for the prescribed input (the same data are required for the quasi-cylindrical approximation method of Hall (see II)). The amplitude of a trapped wave is uniquely determined by the tube geometry and the Reynolds number, and it is found to be necessarily large. The following results are found (see figure 1).

(*a*) The flow is supercritical upstream of breakdown and subcritical downstream. This is consistent with all known experiments.

(*b*) A stationary wave may occur only if the tube diverges in the direction of flow, i.e. if an adverse pressure gradient exists on the axis. If the tube contracts (favourable pressure gradient) no stationary waves are possible. This is consistent with all experiments.

(*c*) A closed streamline representing the boundary of the trapped wave, or recirculating vortex breakdown eddy, is approximately the same size as that observed by Sarpkaya (III).

(*d*) The wall pressure behaviour observed by Sarpkaya (III) and by Kirkpatrick (1965) is qualitatively reproduced.

(*e*) The calculated position of the breakdown depends upon Reynolds number, and the calculated position as a function of Reynolds number agrees well with

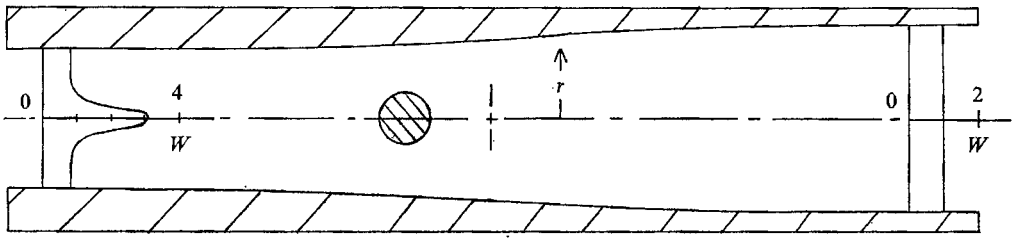

FIGURE 1. Schematic view of a vortex breakdown at Reynolds number of 6000 based upon mean axial velocity and tube diameter.

III (figure 2). As the Reynolds number increases, the breakdown is driven upstream, and for high Reynolds number, it must be located near to, or partly inside, the portion of minimum duct area. Kirkpatrick's (1965) and Harvey's (1962) experiments were at higher Reynolds number than those in III, and the locations of the breakdowns observed are consistent with our findings.

Criticism

The principal criticism to be made of the proposal has already been set out by Hall (II), who points out that vortex breakdown is a strongly nonlinear phenomenon, so that the present wave calculations, and those of previous workers, do not represent a logically consistent explanation. The hypothesis that a strongly nonlinear wave exists that is related to those of small amplitude requires a leap of faith. Unreported work by Leibovich suggests, however, that wave motions of the form proposed here but of arbitrary amplitude may be possible. These are non-dispersive and are analogous to those from the Airy shallow-water theory: they are of the form $\psi = \phi(r)\,A(z,t)$, where ψ is the stream function. Here A satisfies $A_t + c_0 A A_z = 0$. The ordinary differential equations for ϕ are nonlinear and singular at the boundaries and are therefore difficult to treat. In the stationary case $c_0 = 0$, however, an explicit solution is known. See the citation of a communication by Trustrum in Pritchard (1969, p. 457).)

We note that any consistent theory that is valid in the vicinity of the breakdown must reproduce the experimentally observed wall pressure behaviour (*d*). Therefore no great claims are advanced by obtaining the correct trends, since this follows from a diverging duct simply as a consequence of the Bernoulli theorem coupled with the fact that the breakdown partially blocks the duct.

A shortcoming of the proposal is that reversed swirl velocities occur inside the streamline dividing the recirculating breakdown from the flow originating upstream. The model is therefore inadequate to describe the flow inside the breakdown, even though the behaviour of the axial velocity appears to be a promising rough approximation. It has been claimed (Bossel 1969) that reversal of the swirl velocity is a possibility, but this is clearly impossible for an essentially steady axially symmetric flow. Reversed swirl is predicted by inviscid models, however, as in the cited paper by Bossel. The circulation Γ is constant along streamlines in steady flow and if the vortex is chosen to simulate real vortices far upstream one must have $\Gamma \sim \psi$ near the symmetry axis (on which

$\psi = 0$). Since the boundary of the bubble is also $\psi = 0$, reversed swirl must occur inside the bubble when the same functional form for Γ is used everywhere. (This choice of Γ is not required, however. See Leibovich (1968) for an example.) Reversed swirl is not allowed, however, because it requires a means of supplying a 'reversed' torque in a fluid of non-zero viscosity. Furthermore, such flows are also unstable according to the stability criteria of Howard & Gupta (1962). We therefore conclude that the flow in the interior of a breakdown is controlled by viscosity if laminar or by turbulent Reynolds's stresses if turbulent.

We conclude these extended introductory remarks by pointing out that the equations used in the quasi-cylindrical approximation method (which we shall call QC, for short) first advanced by Hall (1965) and further pursued by Bossel (1967) are similar to those used for the present model. The QC model is steady and proceeds, in effect by setting $\kappa = 0$ in the steady form of equations (1) of I. Therefore so far as axial gradients are concerned (of which κ is a measure), this approximation amounts to only the leading term of the long-wave expansions of I and Benjamin (1967). The procedure in applying the QC model is to fix conditions at some axial station, and then compute conditions downstream in the step-by-step fashion familiar in boundary-layer theory. The method is not restricted by the assumptions of small disturbance that apply to the long-wave calculations, but the restrictions on the axial gradients of computed quantities are more severe. When axial gradients begin to grow large in the calculations, the QC approximation is assumed to fail. In a way analogous to the failure of boundary-layer theory at separation, an incipient vortex breakdown is assumed to be the cause of failure. We believe that the analogy with boundary-layer separation is not appropriate, but that the approximation correctly signals breakdown because it simulates the change of the flow from supercritical towards critical. It thus signals the introduction of upstream wave propagation possibilities into the physics. A similar failure would occur in a step-by-step calculation (which is possible) in a supersonic duct flow. If the flow were driven towards sonic conditions, the calculation procedure would fail, exactly as the QC approximation fails. One therefore cannot neglect the overwhelming physical consequences of wave propagation possibilities. We should note further at this point that the very rapid drop from a supercritical state is consistent with the presence of a large amplitude wave, which is expected to decay exponentially fast both upstream and downstream.

The remainder of this paper is devoted to establishing results (*a*)–(*e*) above.

2. Specification of the problem

We assume familiarity with the formulation of I. The duct (dimensionless) wall is described by the equation

$$Y = 1 + \delta h(x), \tag{1}$$

the stream function (to lowest order in the quantities δ, ϵ and α) in critical flow is

$$\Psi = \frac{1}{2}\int_0^y W\,dy + \phi_0(y)\,[\delta^{\frac{1}{2}} f(x) + \epsilon A(z,t)] \tag{2}$$

and the 'circulation' is

$$\Gamma = \Gamma_s(y) + \gamma_0(y)\,[\delta^{\frac{1}{2}} f(x) + \epsilon A(z,t)], \tag{3}$$

where A is governed by the equation

$$A_t = \epsilon[c_1 A A_z + c_2 A_{zzz}] + \delta^{\frac{1}{2}} c_1 (fA)_z + c_5 \tilde{\mu} A \tag{4}$$

(see I, equation (18)).

The function $f(x)$ is related to the wall shape by

$$ff_x = \omega_1 h_x,$$

where the formula determining ω_1 is given in I, equation (11). To be definite, we assume that $0 \leqslant h \leqslant 1$, and therefore (since ω_1 will be shown to be negative for Sarpkaya's (1971) experiments) take

$$f = [2\omega_1(h-1)]^{\frac{1}{2}}. \tag{5}$$

Equations for the constants c_1 and c_2 appearing in (4) are given in I, while the formula for c_5 is given in Leibovich & Randall (1971) (where one must replace c_3 by c_5 to translate the notation to that of the present paper).

The functions $W(y)$, $\Gamma_s(y)$ and $h(x)$ are assumed to be given. To simulate the experiments of III, we select $W = 1$ and

$$\Gamma_s = K(1 - e^{-14y}) \tag{6}$$

and in order for this flow to be critical as required here $K = 0{\cdot}4323$. (This represents a slight departure from our normalization of velocities. Here velocities are referred to the axial velocity rather than to the maximum swirl velocity. It makes little difference to the numerical values, since the maximum swirl in critical flow for this vortex is 1·03.) The form of (6) and the factor of 14 in the exponent are obtained from the measurements in III (and also from Harvey 1962). The value of K is obtained by numerically solving equation (7) of I for the critical case $c_0 = 0$. It may also be inferred from calculations in Leibovich (1970, p. 810, where a misprint must be corrected: $K = \kappa_0 \alpha^{-\frac{1}{2}}$, and κ_0^2 in (16) should be replaced by κ_0). Sarpkaya's (III) swirl parameter Ω is roughly related to K by the equation $\Omega = \pi K$, so we deal with $\Omega \doteqdot 1{\cdot}36$.

Sarpkaya's test section consisted of a conically tapered tube joined (at the upstream end) to a rounded throat 1·5 in. in diameter. The downstream end was connected to a straight tube 2 in. in diameter, and the tapered tube was 10 in. in length. Therefore, the area change parameter

$$\delta = \left(\frac{\text{max diameter}}{\text{min diameter}}\right)^2 - 1 = \tfrac{7}{9}.$$

Our computer solutions of (4) for the wave shape are of initial-value type with initial data given on the entire real z axis. A convenient analytical representation of the wall variation $h(x)$ suitable for all $|z| < \infty$ that could provide a reasonable approximation to the diverging portion of Sarpkaya's tube was desired. The profile chosen was

$$h(x) = h(\alpha z) = \tfrac{1}{2}[1 + \tanh(\alpha \epsilon^{\frac{1}{2}} z'/b)], \tag{7}$$

where b is the minimum (dimensional) tube radius and z' is the dimensional axial distance. For convenience, we write $z_b = z'/b$. The centre of the test section was chosen as the origin for z_b, and the parameter $\alpha\epsilon^{\frac{1}{2}}$ in (7) was fixed by setting $h = 0{\cdot}99$ at $z_b = 6{\cdot}67$, so that $\alpha\epsilon^{\frac{1}{2}} = 0{\cdot}3445$. Other wall representations were tried, and the position of breakdown was found to be sensitive to the wall shape. The results obtained are given by Randall (1972).

3. Heuristic consideration of the location of trapped waves

In I it is shown that an equation of the form (4) may describe wave amplification due to geometrical constraints, and dissipation due to viscosity as described by the last term in (4) is also present. A stationary wave in equilibrium is a possible outcome of the competition between amplification and dissipative effects, and such a 'trapped wave' (since the analysis shows that equilibrium is possible only at certain locations) is sought here.

A good approximation to the possible locations of trapped waves can be found by considering the wave momentum M and energy E, where

$$M(t) = \int_{-\infty}^{\infty} A\,dz, \quad E(t) = \frac{1}{2}\int_{-\infty}^{\infty} A^2\,dz.$$

Integration of (4) shows that, if $A \to 0$ as $|z| \to \infty$,

$$M = M_0 e^{\tilde{\mu}c_5 t}, \tag{8}$$

where M_0 is the initial momentum. Since $c_5 < 0$, $M \to 0$ as t increases. This does not necessarily imply $|A| \to 0$ everywhere, of course. By multiplying (4) by A and integrating by parts, we find that the rate of change of energy is

$$\frac{dE}{dt} = \int_{-\infty}^{\infty} [\alpha\delta^{\frac{1}{2}}c_1 f_x + 2\tilde{\mu}c_5] \times \tfrac{1}{2}A^2\,dz. \tag{9}$$

The coefficients of $\frac{1}{2}A^2$ varies slowly with z. If A is highly localized, as in a solitary wave, we expect that a good estimate of the wave equilibrium position z_e may be found by setting

$$\alpha\delta^{\frac{1}{2}}c_1 f_x(\alpha z_e) + 2\tilde{\mu}c_5 = 0. \tag{10}$$

The assumptions leading to (10) and the accuracy of its predictions must be verified by a complete transient analysis of the wave motion. It will be seen later that (10) is well supported by such a study.

The following coefficients were computed (see Randall 1972) for the vortex of § 2 to simulate the experiments of III and Harvey (1962):

$$c_1 = -0{\cdot}3838, \quad c_2 = 0{\cdot}0162, \quad c_5 = -96{\cdot}631, \quad \omega_1 = -2{\cdot}8314.$$

Therefore a solution of (10) is possible only if $f_x < 0$, and since $\omega_1 < 0$, this can occur only for a tube diverging in the flow direction.

Figure 2 was constructed from (10) using these results and the parameters of § 2, together with the corresponding results from Sarpkaya's paper (III). The agreement is encouraging.

The speed of a finite amplitude wave depends upon wave amplitude. Therefore

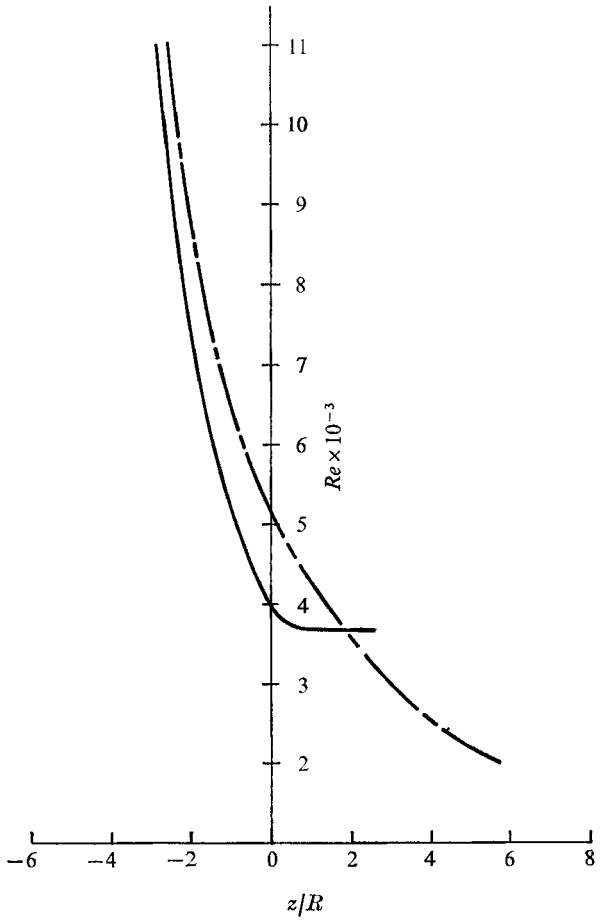

FIGURE 2. Wave equilibrium position, measured from centre of flaring region, *vs.* Reynolds number. — — —, taken from Sarpkaya's (1970) data; ——, predicted by present model.

such a wave will not come to rest at the equilibrium position unless it has the 'correct' amplitude, a_e. Write (4) in the form

$$A_t = c_1\delta^{\frac{1}{2}}fA_z + \epsilon[c_1AA_z + c_2A_{zzz}] + [\alpha\delta^{\frac{1}{2}}c_1f_x + \tilde{\mu}c_5]A$$

and consider its behaviour in the vicinity of equilibrium. If we suppose f to be replaced by its value f_e at equilibrium, the first term on the right is seen to cause a translation at the constant speed $-c_1\delta^{\frac{1}{2}}f_e$. The last term represents amplification or decay which, at equilibrium, should vanish. Neglecting the last term then, the equation is that of Korteweg & de Vries (1895), and it has the localized solution

$$A = a_e\,\mathrm{sech}^2\left\{\left[\frac{c_1a_e}{12c_2}\right]^{\frac{1}{2}}[z - z_e + st]\right\}, \tag{11}$$

where

$$s = \tfrac{1}{3}\epsilon a_e c_1 + c_1\delta^{\frac{1}{2}}f_e \tag{12}$$

and a_e is the constant wave amplitude. It will be seen later that the solitary

wave (11) conforms closely with computer solutions of (4) for large time. If the wave is to remain fixed, $s = 0$, or

$$\epsilon a_e = -3\delta^{\frac{1}{2}} f_e. \tag{13}$$

In a tube that is initially straight, then flares out and becomes straight again as one advances in the direction of the flow, f_x decreases from zero to a minimum and then increases to zero again. As long as

$$\max[-f_x] > 2c_5\tilde{\mu}/c_1\alpha\delta^{\frac{1}{2}} \tag{14}$$

equation (10) has two real solutions. Only the upstream solution is stable, however, in the sense that waves passing through it experience a restoring tendency owing to the amplitude–speed behaviour of nonlinear waves. Upstream of the forward equilibrium point waves decay, while downstream of it they amplify. The (downstream) equilibrium point is unstable for analogous reasons since amplification occurs upstream and decay downstream. If the inequality (14) is not satisfied, wave decay occurs everywhere, and no equilibrium is possible.

Using parameters corresponding to Sarpkaya's (1971) experiment, the plot of equilibrium wave amplitude versus Reynolds number shown in figure 3 was obtained. As one can see, these amplitudes are quite large, too large in fact for the theory leading to (4) to be valid since it requires that the amplitudes be small. As was pointed out by Leibovich (1970), one has to use a large amplitude theory to model vortex breakdown with a solitary wave in order to obtain the zones of recirculation that are observed. Thus the small amplitude analysis does not supply a self-consistent theory. Nevertheless, it does provide a useful model containing all of the important effects of wave steepening due to nonlinearity, of dispersion and of the influence of tube geometry on wave speed and amplification, and the influence of dissipation on wave decay.

4. Numerical solutions for trapped waves

Calculations of solutions of (4) using the parameters of §§ 2 and 3 have been carried out in order to test the heuristic considerations discussed above. The preliminary transformation $T = \epsilon t$ was used. The initial-value problem was solved

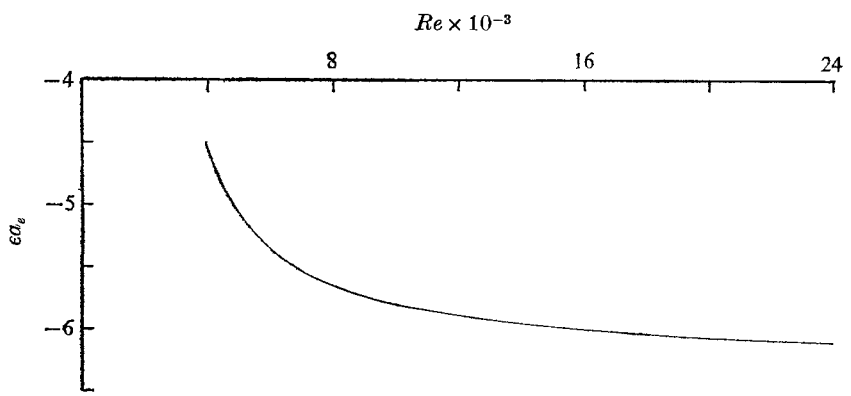

FIGURE 3. Equilibrium wave amplitude *vs.* Reynolds number corresponding to figure 2.

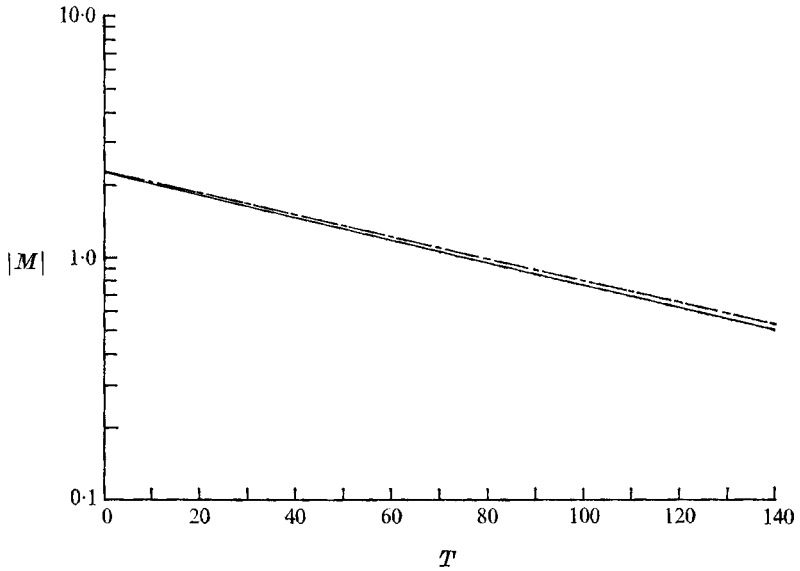

FIGURE 4. Absolute value of wave momentum *vs.* time for waves governed by equation (4), with $A(z, 0)$ given by (15); $Re = 6000$. — — —, correct momentum; ——, computed momentum.

for several different initial conditions using the numerical algorithm given in the appendix. In order to reduce computing time, the heuristic equilibrium values of amplitude and equilibrium position were used as guides in selecting initial data. For the purposes of illustration, the Reynolds number throughout the remaining discussion will be assumed to be 6000, for which the equilibrium amplitude ϵa_e is $-5{\cdot}3712$. For $t = \infty$, the parameter ϵa_e determines the magnitude of the flow disturbance, and it is uniquely fixed in terms of the Reynolds number and tube geometry by (13) and (10). The choice of ϵ or a_e separately, however, is arbitrary owing to the arbitrary distinction made between them in the theory (see Leibovich 1970); once one of these quantities has been chosen, α will also be fixed. Two practical requirements have to be met when choosing ϵ and a_e. One must have ϵ small enough to give a fast momentum relaxation and a_e should not be so large that poor spatial resolution of the numerically determined wave pattern results. In the interest of avoiding prohibitive computing expense while obtaining accurate results, a_e was chosen to $-2{\cdot}5$, fixing ϵ and α at $2{\cdot}1485$ and $0{\cdot}2350$, so that z_e is $-2{\cdot}0925$. The equation describing the first initial distribution to be discussed is

$$A(z, 0) = a_e \operatorname{sech}^2\{[c_1 a_e/12c_2]^{\frac{1}{2}}(z - z_e)\}. \tag{15}$$

The computation using (15) as the initial wave distribution was run until it was apparent that solitary-wave trapping was indeed occurring. As a check on the accuracy of the numerical solution, the wave momentum of the numerically determined wave pattern was monitored periodically and this was compared with the exact momentum decay, as shown in figure 4; the disagreement between the two curves is never more than 2%, which is what one should expect for the

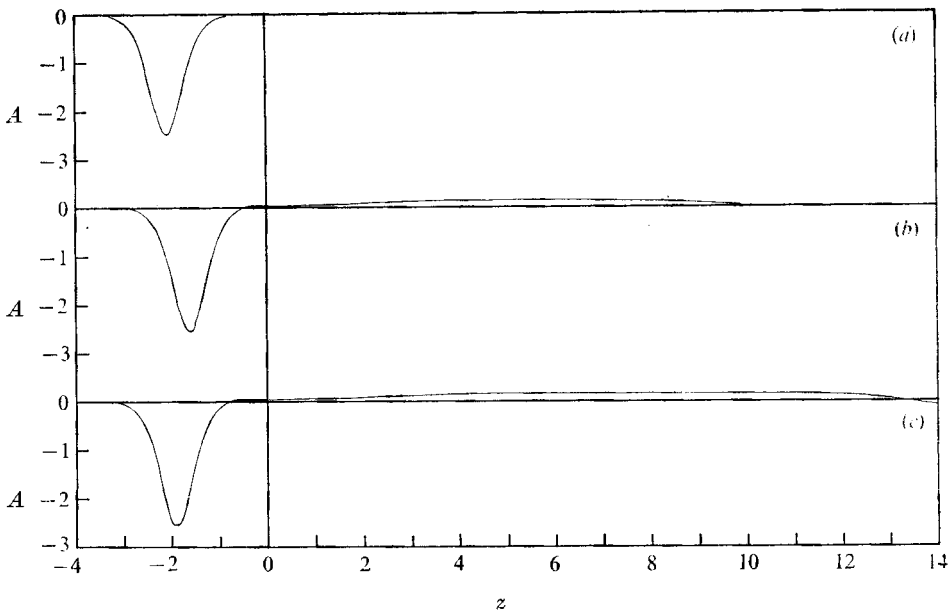

FIGURE 5. Evolution of solitary wave governed by equation (4), corresponding to figure 4. (*a*) $T = 0$. (*b*) $T = 61{\cdot}7$. (*c*) $T = 123{\cdot}4$.

grid spacings being used here. Figure 5 shows the computed wave evolution; figure 6 shows the trajectories of the minimum of the solitary wave developing in figure 5, the leftmost non-zero maximum and the minima of the small oscillations accompanying the solitary wave (which nearly always occur in solitary-wave evolution governed by the Korteweg–de Vries equation (Zabusky 1968)) and figure 7 shows how the energy of the evolved wave pattern varies with time.

Since the wave distribution must undergo momentum decay, the initial solitary-wave distribution must lose momentum. This caused its amplitude to decrease so that the solitary wave shifted to the right and the entire wave distribution suffered an initial loss of energy. Owing to this rightward motion, the solitary wave entered an amplification zone in the tube causing its amplitude to increase, and the energy of the wave distribution started to increase. After sufficient amplification, the centre of the solitary wave moved back very slowly to the left and came to rest about 0·25 axial units to the right of its initial position. While this was happening, the requisite momentum decay was accomplished by the generation of a positive shelf which stretched between the right-hand tail of the solitary wave and the train of small oscillations moving to the right; the energy of the wave distribution increased with time at a decelerating rate and, when the computation was terminated, the energy appeared to be approaching a constant. The solitary-wave amplitude is $-2{\cdot}57$ and its form is very close to that of a Korteweg–de Vries solitary wave with the same amplitude, as shown in figure 8.

With the initial distribution used in the computation just discussed, wave trapping occurs rapidly because the initial condition is almost identical to the

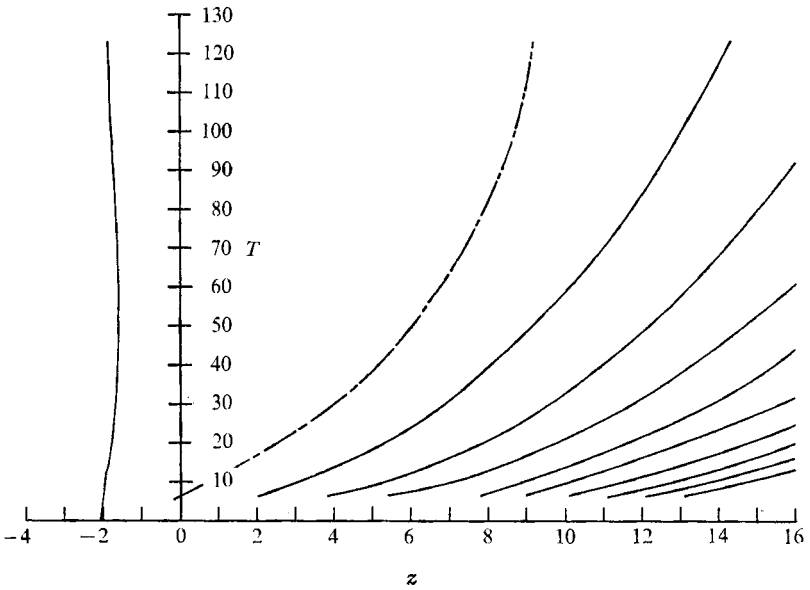

FIGURE 6. Trajectories of minima for wave evolution in figure 5 (solid curves). Broken curve is trajectory of leftmost positive maximum.

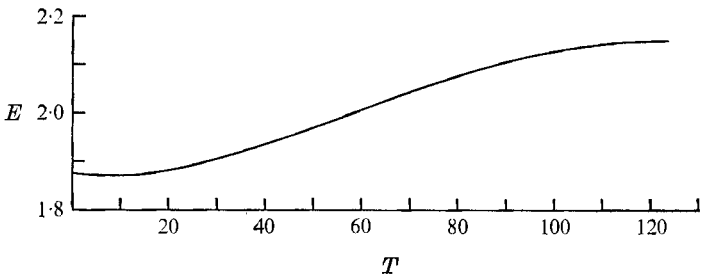

FIGURE 7. Wave energy *vs.* time for wave evolution in figure 5.

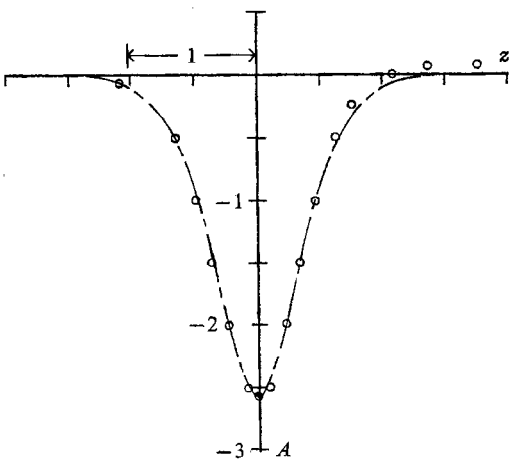

FIGURE 8. Solitary-wave forms. ——, Korteweg–de Vries profile with $a = -2{\cdot}57$; ○, final solitary-wave profile in figure 5.

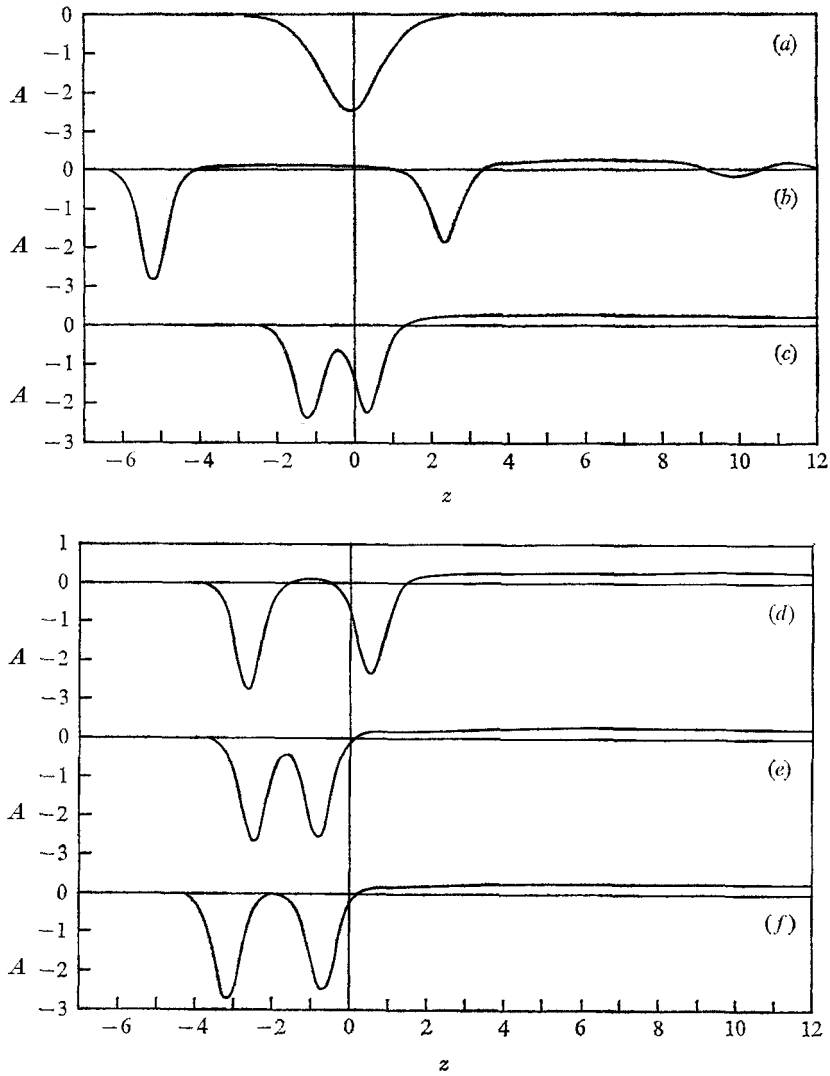

FIGURE 9. For legend see facing page.

expected final form. In order to see whether other initial data may lead to trapping the initial condition (15) was shifted and the following distribution was considered:

$$A(z, 0) = -2{\cdot}5\,\mathrm{sech}^2(z - z_e - 2). \tag{16}$$

When this initial distribution is used with the Korteweg–de Vries equation, two permanent left-moving solitary waves will evolve, with the larger one always leading the smaller one (Zabusky 1968). In view of this and the computation just discussed, one can gain some idea of the initial evolution period when (4) is solved with (16) as initial data. Since the initial distribution is concentrated in an amplification zone, the wave energy will undergo an initial increase. The initial distribution is expected to degenerate into two solitary waves, a large one which

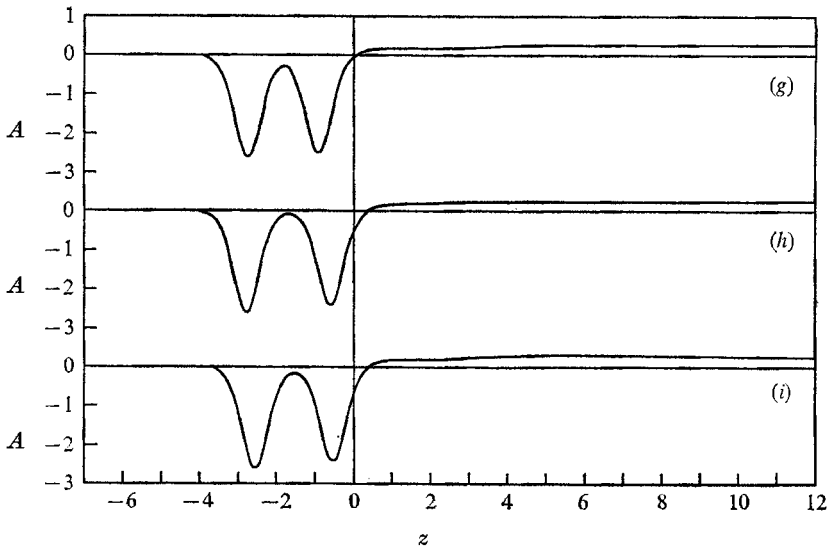

FIGURE 9. Evolution of solitary waves governed by equation (4). $A(z, 0)$ given by (16); $Re = 6000$. (*a*) $T = 0$. (*b*) $T = 54{\cdot}0$. (*c*) $T = 131{\cdot}1$. (*d*) $T = 177{\cdot}4$. (*e*) $T = 223{\cdot}7$. (*f*) $T = 258{\cdot}4$. (*g*) $T = 293{\cdot}1$. (*h*) $T = 327{\cdot}8$. (*i*) $T = 362{\cdot}5$.

will move to the left into the decay zone left of the equilibrium position and a smaller one which initially should move to the right because of its small amplitude. The leftward-moving solitary wave is expected to decay, lose amplitude and be swept back to the right while the right one is expected to amplify and eventually reverse direction and move to the left. This will result in a collision of the two solitary waves and a nonlinear interaction between them that cannot be guessed without computation.

Figure 9 shows the wave evolution from the initial distribution given by (16); figure 10 shows the trajectories of the minima of the two solitary waves, the leftmost positive maximum, and the minima of the small right-moving oscillations accompanying the solitary-wave evolution. Figure 11 shows the wave energy as a function of time. The initial solitary-wave development proceeded as expected, and the wave energy showed the anticipated initial increase. Owing to the decay of the initially larger, left solitary wave, the energy growth rate decreased. While the left solitary wave was decaying, the right one was amplifying and soon became large enough to cause the wave energy to increase again. The first interaction of the solitary waves occurred to the right of the equilibrium position. There was an exchange of energy between the two waves in which the left one gained energy at the expense of the right one, causing them to move apart again. The right solitary wave moved only a short distance to the right before moving back to the left again. In the meantime the left solitary wave moved back into the decay zone, so that by the time the next collision occurred, the centres of the two solitary waves were at approximately equal distances on either side of the equilibrium position. The left solitary wave gained energy from the right one again and a cyclic process began in which the two waves would periodically collide and move apart. Three of these cycles were observed before

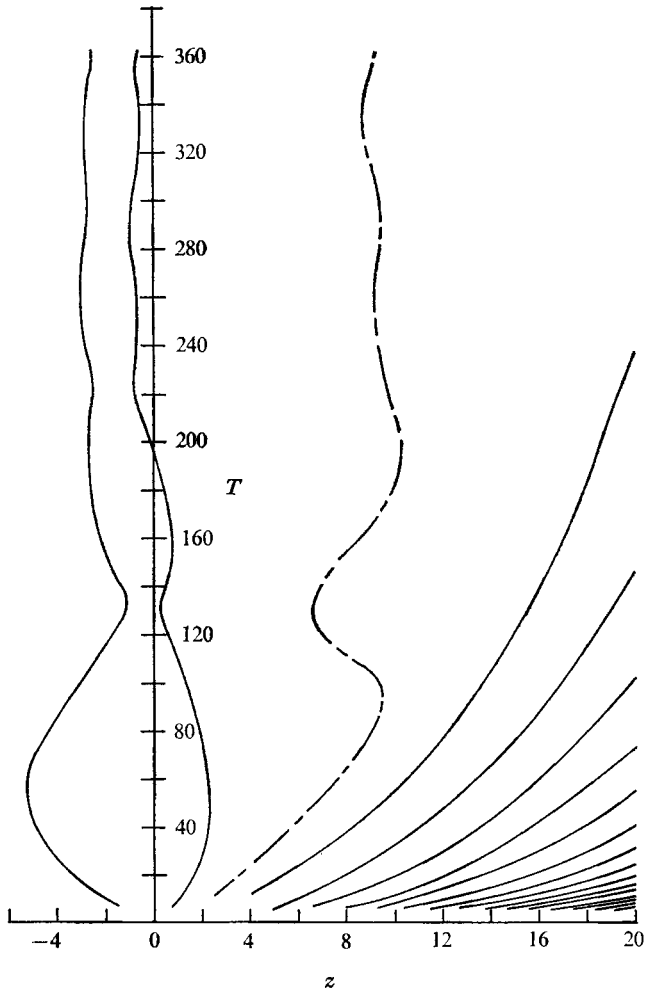

FIGURE 10. Trajectories of minima for wave evolution of figure 9 (solid curves). Broken curve is trajectory of leftmost positive maximum.

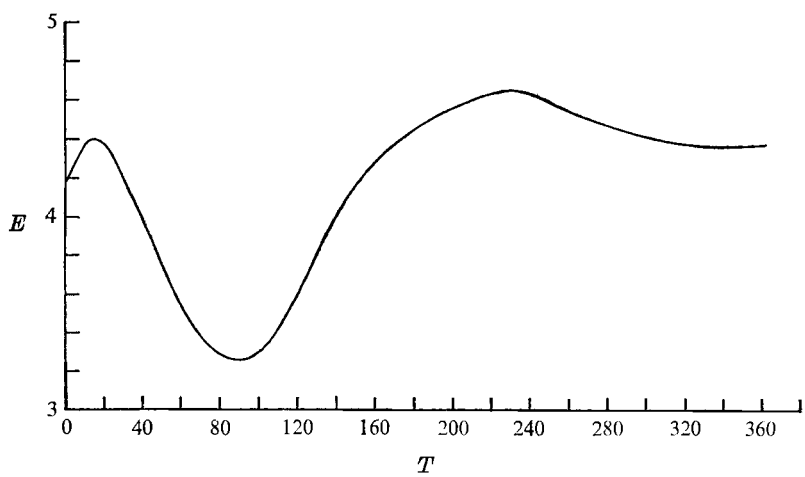

FIGURE 11. Wave energy *vs.* time for wave evolution in figure 9.

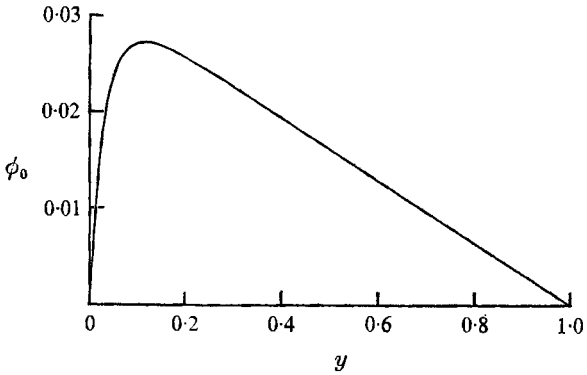

FIGURE 12. Eigenfunction $\phi_0(y)$ for the vortex (6) of § 2.

the computation was terminated. Once the cycles had started, the oscillations of the wave energy became much less severe. As before, the required momentum decay was accommodated by a long positive shelf between the right solitary wave and the small right-moving oscillations.

5. The ultimate steady vortex breakdown flow

Figure 12 shows the eigenfunction $\phi_0(y)$ corresponding to $W = 1$ and the vortex (6). From this result, equation (5) and the parameters ϵ, α and δ appropriate to Sarpkaya's experiment as discussed in §§ 2 and 3, a stationary-wave distribution A may be found and a steady flow field may then be constructed from (2) and (3).

Of the two steady distributions of A obtained in § 4, the first one is chosen for the model. Pairs of axisymmetric vortex breakdowns have never been observed in a variable-area tube; only single (steady) breakdowns have been observed. Single breakdowns may be selected in diverging tubes since the initial development consists of an upstream journey through a zone of decay. The wave motion thus passes through a filter. Presumably only the dominant downstream disturbance can survive to reach a point of stable equilibrium. Boundary-layer displacement effects may also play a role in selecting single trapped waves by shaping the (nominal) duct wall.

The streamline pattern in the neighbourhood of the breakdown constructed from figures 5 and 12 is shown in figure 13. The axial and radial co-ordinates in figure 13 are both referred to the tube radius scale b. As one can see from this figure, the theory predicts a well-defined cell of recirculating fluid which is symmetrical around the tube centre-line and occurs in the neighbourhood of the equilibrium position.

In his 1970 report, Sarpkaya presents a sketch of the contour of a 'representative breakdown bubble' which spans an axial distance of about 0·75 tube radii and a radial distance of about 0·32 tube radii (see II, figure 7). Considering that a small disturbance theory is being used to model a large disturbance phenomenon the agreement between Sarpkaya's sketch and figure 13 is quite good. Sarpkaya's bubble is more elongated and less symmetrical in the axial direction than the

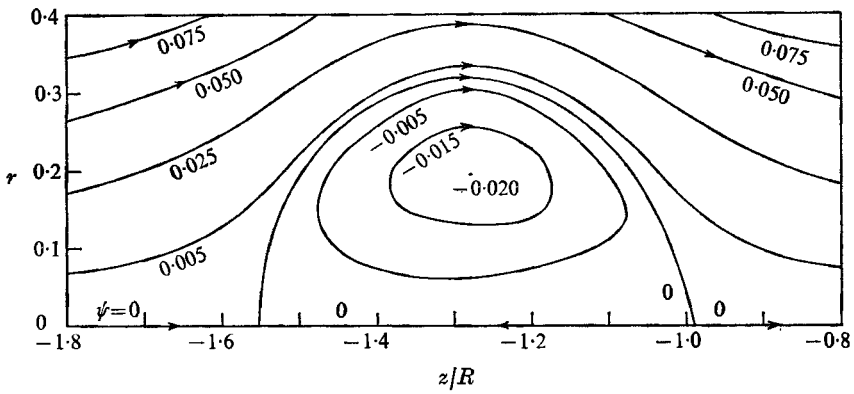

FIGURE 13. Streamline pattern in neighbourhood of equilibrium position using final wave profile in figure 5 and radial structure function in figure 12. Numbers next to streamlines are stream-function values.

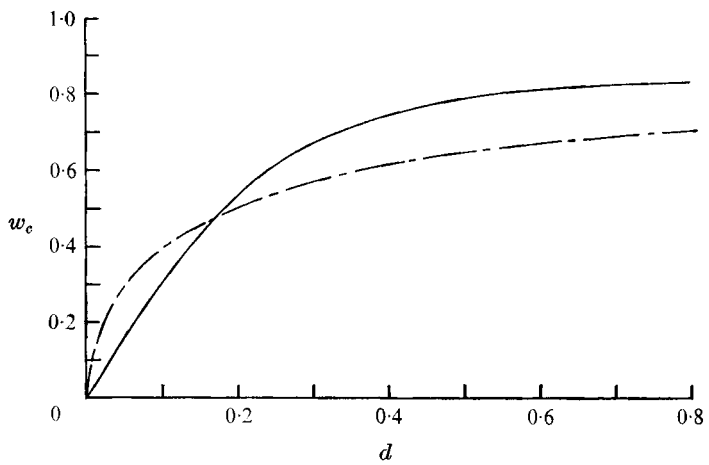

FIGURE 14. w_c = centre-line axial velocity/far upstream centre-line axial velocity. d = distance, in tube radii, upstream of vortex breakdown nose in figure 13. ——, theory; — — —, representative of Sarpkaya's (1970) observations.

bubble predicted here and it has no rear stagnation point because fluid empties out of the rear of the bubble and spirals away in a non-axisymmetric manner. This, of course, is a feature that the nearly inviscid, axisymmetric model cannot predict. The small right-moving oscillations observed in the solitary-wave computations are much too small to account for the periodic motion that occurs behind the observed breakdown bubbles.

Figure 14 is a plot of the centre-line axial velocity normalized with respect to its undisturbed value far upstream as a function of the axial distance upstream of the breakdown. The solid curve is the theoretically predicted one and the broken curve is representative of Sarpkaya's observations. Not only are the basic trends the same, but the numerical values are close. Sarpkaya's swirl-angle measurements were made 'a short distance ahead of the breakdown'. The

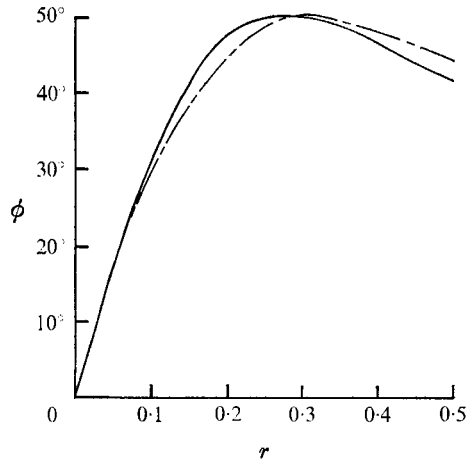

FIGURE 15. Swirl angle (ϕ) *vs.* radius just upstream of breakdown region in figure 13. ——, theory; — — —, Sarpkaya (1970).

theoretical (solid) curve of swirl angle versus tube radius in figure 15 was obtained by taking the inverse tangent of the ratio of swirl velocity (Γ/r) to axial velocity ($2\Psi_y$) just upstream of the calculated bubble shown in figure 13.

Wall pressure measurements by Sarpkaya (III) and Kirkpatrick (1965) are presented in terms of a pressure excess ratio $(p-p_u)/\frac{1}{2}\rho\mathscr{W}^2$, where p_u is the pressure far upstream of breakdown and $\mathscr{W}$ is the mean axial velocity there. Moving downstream from the upstream region, the pressure excess ratio is initially zero but increases slowly as one approaches the breakdown, where it reaches a local maximum, decreases rapidly through the breakdown region and then slowly increases to a final constant value in the downstream region. Using the present model, one can find with the aid of Bernoulli's equation that the first-order estimate of the pressure excess ratio is given by

$$(p-p_u)/\tfrac{1}{2}\rho\mathscr{W}^2 = 2\phi_0'(1)\,[\delta^{\frac{1}{2}}(f^- - f) - \epsilon A], \tag{17}$$

where $f^- = f(-\infty)$. Equation (5) indicates that f^- is the largest value of f and one can see from figure 12 that $\phi_0'(1)$ is negative. Therefore (17) predicts that the pressure excess ratio far upstream vanishes, and changes most rapidly in the neighbourhood of the breakdown, where A varies much faster than f. It is generally negative downstream, however, and this does not agree with observation. The discrepancy may be traced to the fact that deceleration due to the divergence of the tube, which is of $O(\delta)$, is not accounted for in (2) and (3). The $O(\delta)$ term in the stream function is $\delta h\theta_1(y)$, and when this term is included in the pressure excess equation, one finds that

$$(p-p_u)/\tfrac{1}{2}\rho\mathscr{W}^2 = 2\phi_0'(1)\,[\delta^{\frac{1}{2}}(f^- - f) - \epsilon A] - 2\delta h\theta_1'(1). \tag{18}$$

$\phi_0'(1)$ has a small numerical value and $O(\delta)$ terms involving it are neglected in this equation. The numerical value of $\theta_1'(1)$ is $-1{\cdot}15$. With this modification, the calculated pressure is in qualitative agreement with experiment, as one may

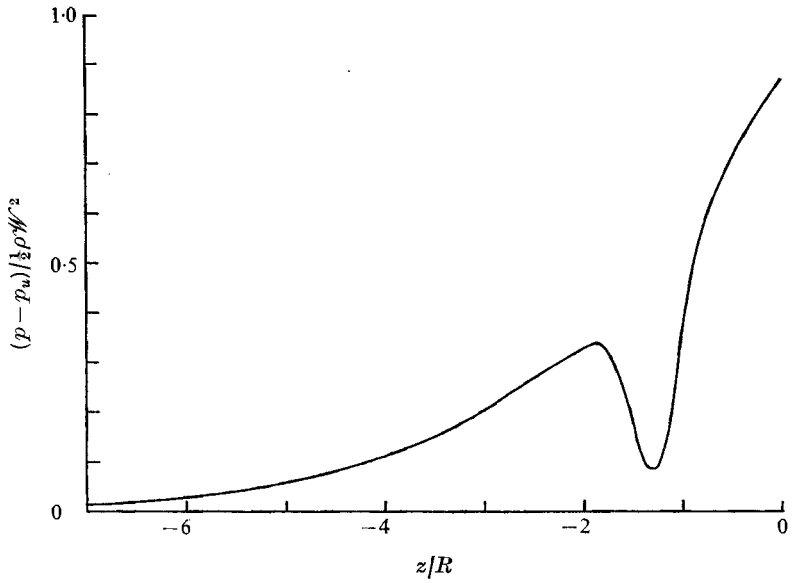

FIGURE 16. Wall pressure distribution caused by vortex breakdown in a diverging tube, calculated from the present model.

see from figure 16, but exhibits a highly exaggerated response to the presence of a trapped wave.

By varying the Burgers vortex exponent in (6), one can vary the swirl parameter K (or Ω) and obtain a family of equilibrium position curves similar to those in figure 2. As shown by Randall (1972), choosing smaller values of the exponent results in larger values of K and this shifts the equilibrium position curve to the left. Sarpkaya (III) observed similar trends. The theory would also predict a family of swirl-angle curves similar to figure 15, but for axisymmetric vortex breakdowns, Sarpkaya obtained only one such curve for all the values of Ω generated. The discrepancy is most likely due to the fact that the support-flow circulation was chosen arbitrarily with no regard for the influence of viscosity upon the exponent in (6). An analysis of vortex cores by Batchelor (1964) indicates that the exponent is inversely proportional to viscosity. The present model does not allow for this.

As one can see from figure 13, reversed axial velocities occur inside the breakdown bubble as indeed they must in order to form the cell of recirculating fluid. Figure 17 shows a plot of the most severe radial variations of axial velocity taken on the plane perpendicular to the tube axis near the eye of the bubble, using equation (2) and the numerical data. Such flow reversals are an essential feature of vortex breakdown observed experimentally. What is not reported experimentally, however, is the reversal of tangential velocities shown in figure 18, which was obtained using equation (3) at the eye of the computed bubble.

Figure 1 shows an overall view of the flow calculated for $R_e = 6000$. The velocity in the straight section far upstream of the breakdown may be calculated from (2) and (5) to be

$$w = W + 2\theta_0'[2\delta|\omega_1|]^{\frac{1}{2}}$$

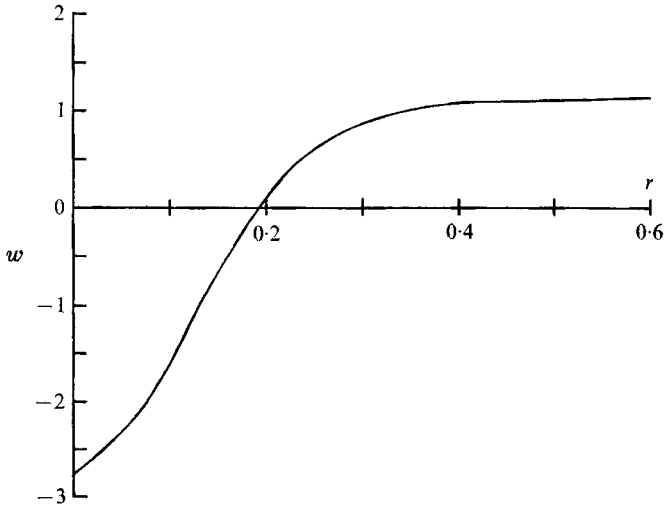

FIGURE 17. Axial velocity *vs.* radius near the eye of the breakdown bubble in figure 13.

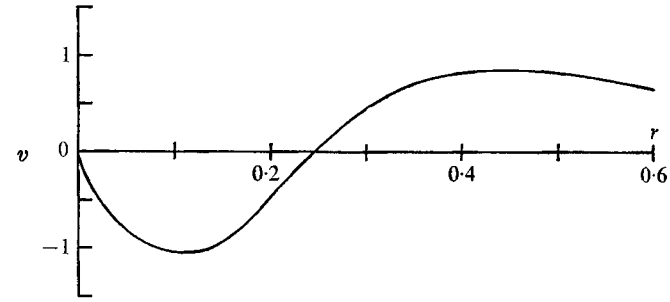

FIGURE 18. Tangential velocity *vs.* radius near the eye of the breakdown bubble in figure 13.

and is supercritical. In the straight section downstream of the breakdown, the $\delta^{\frac{1}{2}}$ contribution vanishes. Deceleration of $O(\delta)$ due to the enlarged tube area occurs, however, and may be found from I to produce the (subcritical) axial velocity

$$w = W + 2\delta\theta_1'(y),$$

where the problem for θ_1 is given in I.

This work was supported by NASA grant NGL-33-010-042, monitored by the Lewis Research Center.

Appendix. Numerical algorithm for solving the wave equation

The numerical procedure for solving (4) involved using the following finite-difference representation of that equation, modelled on one used by Zabusky (1968) for solving the Korteweg–de Vries equation:

$$\begin{aligned}\frac{1}{4h_\tau}&(3A_i^{l+1}-3A_i^l+A_{i-2}^{l+1}-A_{i-2}^l)\\ &=(c_1/4h_z)\,(A_{i+1}^l+A_{i-2}^{l+1})\,(A_{i+1}^l-A_i^{l+1}+A_{i-1}^l-A_{i-2}^{l+1})\\ &\quad+(c_2/h_z^3)\,(A_{i+1}^l-3A_i^l+3A_{i-1}^l+A_{i-2}^l)\\ &\quad+(\delta^{\frac{1}{2}}c_1/2\epsilon h_z)\,(f_{i+1}A_{i+1}^l-f_iA_i^{l+1}+f_{i-1}A_{i-1}^l-f_{i-2}A_{i-2}^{l+1})\\ &\quad+(\tilde{\mu}c_5/4\epsilon)\,(A_{i+1}^l+A_i^{l+1}+A_{i-1}^l+A_{i-2}^{l+1}),\end{aligned}$$

where f_i and A_i^l are the value of f at the ith spatial grid point, the computed value of $A(z,t)$ at the lth time level and ith grid point, and

$$h_\tau=\epsilon(t_{l+1}-t_l)\quad\text{and}\quad h_z=z_{i+1}-z_i.$$

For details of the computational procedure, discussions of errors, and numerical stability see Randall (1972). Owing to the trapping of the solitary waves, the left-hand end of the spatial interval (if it is properly chosen) need not be adjusted as the computation proceeds, but owing to the rightward movement of the small oscillations and the expanding positive shelf between the oscillations and the rightmost solitary wave, the right-hand end of the spatial interval has to be moved to the right occasionally. The amplitude of the oscillations passing through the rightmost grid point was never allowed to be more than 1% of the solitary-wave amplitude. The initial spatial interval was 37 axial units long, running from -7 to 30.

The spatial grid size used in the computations discussed in this paper was 0·1 and the temporal grid size was assigned its maximum allowable value for numerical stability:

$$h_\tau=\tfrac{1}{4}c_2^{-1}h_z^3=0{\cdot}01543.$$

REFERENCES

Batchelor, G. K. 1964 Axial flow in trailing line vortices. *J. Fluid Mech.* **20**, 645.

Benjamin, T. B. 1962 Theory of the vortex breakdown phenomenon. *J. Fluid Mech.* **14**, 593.

Benjamin, T. B. 1967 Some developments in the theory of vortex breakdown. *J. Fluid Mech.* **28**, 65.

Bossel, H. H. 1967 Inviscid and viscous models of the vortex breakdown phenomenon. Ph.D. thesis, University of California, Berkeley.

Bossel, H. H. 1969 Vortex breakdown flowfield, *Phys. Fluids*, **12**, 498.

Hall, M. G. 1965 A numerical method for solving the equations for a vortex core. *Aero. Res. Counc. R. & M.* no. 3467.

Hall, M. G. 1972 Vortex breakdown. *Ann. Rev. Fluid Mech.* **4**, 195.

Harvey, J. K. 1962 Some observations of the vortex breakdown phenomenon. *J. Fluid Mech.* **14**, 585.

HOWARD, L. N. & GUPTA, A. S. 1962 On the hydrodynamic and hydromagnetic stability of swirling flows. *J. Fluid Mech.* **14**, 463.

KIRKPATRICK, D. L. I. 1965 Experimental investigations of the breakdown of a vortex in a tube. *Aero. Res. Counc. Current Paper*, no. 821.

KORTEWEG, D. J. & DE VRIES, G. 1895 On the change of form of long waves advancing in a rectangular canal, and on a new type of long stationary waves. *Phil. Mag.* **39** (5), 422.

LEIBOVICH, S. 1968 Axially-symmetric eddies embedded in a rotational stream. *J. Fluid Mech.* **32**, 529.

LEIBOVICH, S. 1969 Wave motion and vortex breakdown. *A.I.A.A. Paper*, no. 69–645.

LEIBOVICH, S. 1970 Weakly non-linear waves in rotating fluids. *J. Fluid Mech.* **42**, 803.

LEIBOVICH, S. & RANDALL, J. D. 1971 Dissipative effects on non-linear waves in rotating fluids. *Phys. Fluids*, **14**, 2559.

LEIBOVICH, S. & RANDALL, J. D. 1973 A amplification and decay of long nonlinear waves. *J. Fluid Mech.* **58**, 481.

PRITCHARD, W. G. 1969 The motion generated by a body moving along the axis of a uniformly rotating fluid. *J. Fluid Mech.* **39**, 443.

RANDALL, J. D. 1972 Two studies of solitary wave propagation in rotating fluids. Ph.D. thesis, Cornell University.

SARPKAYA, T. 1970 An experimental investigation of the vortex breakdown phenomenon. *U.S. Naval Postgrad. School. Rep.* NPS-59L0071A.

SARPKAYA, T. 1971 On stationary and travelling vortex breakdowns. *J. Fluid Mech.* **45**, 545.

SQUIRE, H. B. 1962 Analysis of the 'vortex breakdown' phenomenon. In *Mizellaneen du Angewandten Mechanik*. Berlin: Akademie.

ZABUSKY, N. J. 1968 Solitons and bound states of the time-independent Schrödinger equation. *Phys. Rev.* **168**, 124.